A Multifunctional Role of Leucine-Rich α-2-Glycoprotein 1 in Cutaneous Wound Healing Under Normal and Diabetic Conditions

Chenghao Liu,[1] Melissa Hui Yen Teo,[2] Sharon Li Ting Pek,[3] Xiaoting Wu,[4] Mei Ling Leong,[4] Hui Min Tay,[1,5] Han Wei Hou,[1,5] Christiane Ruedl,[4] Stephen E. Moss,[6] John Greenwood,[6] Subramaniam Tavintharan,[3,7,8] Wanjin Hong,[2] and Xiaomeng Wang[1,2,9]

Diabetes 2020;69:2467–2480 | https://doi.org/10.2337/db20-0585

Delayed wound healing is commonly associated with diabetes. It may lead to amputation and death if not treated in a timely fashion. Limited treatments are available partially due to the poor understanding of the complex disease pathophysiology. Here, we investigated the role of leucine-rich α-2-glycoprotein 1 (LRG1) in normal and diabetic wound healing. First, our data showed that LRG1 was significantly increased at the inflammation stage of murine wound healing, and bone marrow–derived cells served as a major source of LRG1. LRG1 deletion causes impaired immune cell infiltration, reepithelialization, and angiogenesis. As a consequence, there is a significant delay in wound closure. On the other hand, LRG1 was markedly induced in diabetic wounds in both humans and mice. LRG1-deficient mice were resistant to diabetes-induced delay in wound repair. We further demonstrated that this could be explained by the mitigation of increased neutrophil extracellular traps (NETs) in diabetic wounds. Mechanistically, LRG1 mediates NETosis in an Akt-dependent manner through TGFβ type I receptor kinase ALK5. Taken together, our studies demonstrated that LRG1 derived from bone marrow cells is required for normal wound healing, revealing a physiological role for this glycoprotein, but that excess LRG1 expression in diabetes is pathogenic and contributes to chronic wound formation.

Wound healing is a natural reparative response to tissue injury. It proceeds through four continuous and overlapping phases: homeostasis, inflammation, proliferation, and tissue remodeling (1). Failure to progress through these phases in an orderly manner leads to impaired wound healing, which represents one of the common causes of morbidity associated with diabetes, affecting ∼25% of individuals with diabetes (2). These wounds frequently serve as portals of entry for bacterial infection that may lead to sepsis and lower-extremity amputation (3). Staggeringly, patients with lower-extremity amputation have a 5-year mortality rate of up to 50% (4). With the rising prevalence of diabetes, the incidence of wound complications is expected to increase substantially, posing a significant socioeconomic burden (5).

A plethora of factors contributes to delayed wound closure in patients with diabetes, such as excessive neutrophil infiltration and activation, impaired angiogenesis, and defective epithelial cell migration and proliferation (6). These defects lock the wound into a self-perpetuating inflammatory stage (7), which causes further tissue injury by increasing the production of inflammatory cytokines, reactive oxygen species, destructive enzymes, and cytotoxic extracellular traps in a process termed NETosis (8) (where NET is neutrophil extracellular trap). Thus, targeting

[1]Lee Kong Chian School of Medicine, Nanyang Technological University, Singapore
[2]Institute of Molecular and Cell Biology, Agency for Science, Technology and Research, Singapore
[3]Clinical Research Unit, Khoo Teck Puat Hospital, Singapore
[4]School of Biological Sciences, Nanyang Technological University, Singapore
[5]School of Mechanical and Aerospace Engineering, Nanyang Technological University, Singapore
[6]Institute of Ophthalmology, University College London, London, U.K.
[7]Diabetes Centre, Admiralty Medical Centre, Singapore
[8]Division of Endocrinology, Department of Medicine, Khoo Teck Puat Hospital, Singapore
[9]Singapore Eye Research Institute, The Academia, Singapore

Corresponding authors: Xiaomeng Wang, wangxiaomeng@ntu.edu.sg, and Wanjin Hong, mcbhwj@imcb.a-star.edu.sg

Received 3 June 2020 and accepted 24 August 2020

This article contains supplementary material online at https://doi.org/10.2337/figshare.12860753.

inflammation serves as an attractive strategy to kick-start the proliferation phase of wound healing and promote repair. A number of anti-inflammatory agents have been developed over the last 20 years (9). Despite effectiveness in promotion of wound closure in rodent models, limited success has been achieved in clinical trials (10). This is likely due to the highly dynamic and complex interactions between different types of cell, extracellular matrix components, and soluble factors present in the wound microenvironment. A better understanding of the molecular mechanisms underlying diabetes-associated healing deficiency will guide the development of more effective therapeutics to treat wounds that do not respond sufficiently to good standard care.

Leucine-rich α-2-glycoprotein 1 (LRG1) is a secreted glycoprotein that was previously reported to regulate pathological neovascularization in the eye by switching the angiostatic TGFβ1-Smad2/3 signaling toward the proangiogenic TGFβ1-Smad1/5/8 signaling in endothelial cells (11). Besides its role in ocular angiogenesis, LRG1 is intimately associated with many inflammatory and autoimmune conditions (12–14) and tumor malignancy (15–17), which shares fundamental molecular mechanisms with chronic wound healing (18). Recently, elevated serum LRG1 levels were reported in patients with diabetes with peripheral arterial disease (19), a major risk factor for diabetic foot ulcers (DFU) (20). Paradoxically, exogenous LRG1 was reported to accelerate wound healing by promoting keratinocyte migration in animal models (21). Here, we characterized LRG1 expression level and pattern in wound tissue, investigated its contribution to wound healing under normal and diabetic condition using *Lrg1*-null mice, and explored its mechanism of action.

RESEARCH DESIGN AND METHODS

Human Sample Analysis

This study was approved by Khoo Teck Puat Hospital Ethics Review Board (NHG Domain Specific Review Board). Adults between 21 and 90 years old with type 2 diabetes seen in Diabetes Centre of Khoo Teck Puat Hospital were enrolled into this study. Fasting blood and debrided tissues were collected from patients with ulcers during their podiatry assessment clinic. Fasting blood samples were centrifuged within 1 h after collection and kept at 4°C during this period. Thereafter, they were stored at −80°C in aliquots and used without additional freeze-thaw cycles. Devitalized tissue was obtained from desloughing and debridement performed as part of usual care. These samples were stored in liquid nitrogen until retrieval for assays described below. Control samples were obtained from patients without type 2 diabetes with venous ulcers in the same clinic. Serum level of LRG1 was measured using an ELISA kit (Immuno-Biological Laboratories, Hamburg, Germany) according to the manufacturer's instructions.

Animals and Induction of Diabetes

C75BL/6J mice were purchased from InVivos (Singapore). *Lrg1*$^{-/-}$ mice were originally generated by the University of California, Davis, Knockout Mouse Project (KOMP) Repository Collection (https://www.komp.org) and were a generous gift from J. Greenwood and S.E. Moss (UCL Institute of Ophthalmology). Animal experiments were performed in compliance with the guidelines of the Institutional Animal Care and Use Committee (ARF-SBS/NIE-A0268/A19036) of Nanyang Technological University and the Guide for Care and Use of Laboratory Animals published by the National Institutes of Health. Diabetes was induced in 6- to 8-week-old male mice by intraperitoneal injection of 50 mg/kg streptozotocin (STZ) (50 mmol/L sodium citrate buffer, pH 4.5) for five consecutive days as previously described (22). Diabetes was confirmed when fasting blood glucose (FBG) was >200 mg/dL.

Creation of Full-Thickness Cutaneous Wounds

Six full-thickness cutaneous wounds were created on mouse dorsal skin using 4-mm Integra Miltex Standard Biopsy Punches (Thermo Fisher Scientific). Wounds were imaged daily with a digital camera. Wound size was quantified with use of ImageJ (National Institutes of Health). We used 6-mm Integra Miltex Standard Biopsy Punches (Thermo Fisher Scientific) for biopsy collection at different time points following injury. The mouse excisional wound splinting model was employed as previously described (23).

Bone Marrow Transplantation

Six-week old mice were irradiated at two doses of 5.5 Gy irradiation using a BIOBEAM GM γ irradiation device (Gamma-Service Medical, Leipzig, Germany). Bone marrow cells (BMCs) from female mice were harvested and filtrated through a 70-μm cell strainer (Falcon). BMCs (3×10^6) were intravenously injected into the irradiated recipient mice through the tail vein 24 h after the irradiation. Eight weeks after reconstitution, wounds were created at flanks of recipient mice.

Isolation and Flow Cytometry Analysis of Myeloid Cells From Wound Tissue

Wound tissues were digested in Iscove's modified Dulbecco's medium (Thermo Fisher Scientific) containing 2% FBS, 2 units/mL DNase I (Roche, Switzerland), and 1 mg/mL collagenase D (Roche) and passed through a 40-mm cell strainer for obtaining single-cell suspension. Red blood cells were lysed using 0.89% NH_4Cl lysis buffer and removed by centrifugation. Cell pellet was resuspended and preincubated with anti–Fc receptor antibody (clone 2.4G2) followed by further incubation with anti-mouse BUV737-labeled CD45 (clone 30-F11), allophycocyanin-Cy7–labeled anti-mouse CD11b (clone M1/70), anti-mouse F4/80 (clone BM8), BUV395-labeled anti-mouse Ly6G (clone 1A8), BV605-labeled anti-mouse Ly6c (clone HK1.4), phycoerythrin-Cy7–labeled anti-mouse CD11c (clone N418), and BV421-labeled anti-mouse I-A/I-E clone (M5/114.15.2). Dead cells were labeled with fixable viability stain 510 (BD Biosciences, San Jose, CA). Cells were then fixed

and permeabilized before being stained with anti–LRG-1 antibody (cat. no. 13224-1-AP; Proteintech) followed by FITC-labeled donkey anti-rabbit IgG (clone Poly4064). Cells were washed and subjected to analysis on a five-laser flow cytometer (BD LSRFortessa; BD Biosciences). Data were analyzed with FlowJo software (TreeStar, Ashland, OR).

Cells and Cell Culture

Primary mouse and human peripheral blood neutrophils (Institutional Review Board of Nanyang Technological University [IRB-2014-04/27]) were isolated, purified, and cultured as previously described (24,25). Human neutrophil-like cells (dHL-60) were derived from human promyelocytic leukemia cell line (HL-60; ATCC) by incubation with 1% DMSO (Sigma-Aldrich) for 7 days. Human dermal microvascular endothelial cells (HDMECs) (PromoCell), normal human dermal fibroblasts (PromoCell), human keratinocyte line HaCaT (ATCC), and Freestyle 293-F cells (Gibco, Thermo Fisher Scientific) were maintained according to the supplier's instruction. Cells were treated with 20 $\mu g\ mL^{-1}$ recombinant human LRG1 (rhLRG1), LDN193189 (100 nmol/L) (Sigma-Aldrich), SB431542 (10 μmol/L) (Sigma-Aldrich), and MK-2206 (10 μmol/L) (Selleck Chemicals) and as indicated.

Histology, Immunohistochemistry, and Immunofluorescence

Mice skin tissues were fixed in 4% paraformaldehyde and embedded in paraffin following a standard protocol. Paraffin sections (5 μm thick) were subjected to staining with hematoxylin-eosin or LRG1 antibody (cat. no. 13224-1-AP; Proteintech). For immunofluorescence staining, skin tissues were embedded in O.C.T. Compound (Thermo Fisher Scientific). Cryopreserved skin sections (5 μm thick) were stained with primary antibodies against LRG1 (13224-1-AP; Proteintech), F4/80 (MCA497; Bio-Rad), CD11b (130-113–235; Miltenyi Biotec), CD31 (550274; BD Biosciences), Myeloperoxidase (MPO) (ab9535; Abcam, Cambridge, U.K.), and Ki67 (ab15580; Abcam) followed by staining with Alexa 488 or Alexa 594 secondary antibodies (Thermo fisher Scientific). Images were captured using Leica DM5500 microscope (Leica Microsystems) or Carl Zeiss LSM 710 confocal microscopy (Zeiss, Berlin, Germany), processed using Adobe Photoshop CS6, and analyzed using ImageJ by investigators who were blinded to the identity of the experimental groups.

Quantitative Real-time PCR

Total RNA was extracted and purified with RNAzol RT (cat. no. 888-841-0900; Molecular Research Center) before being reverse transcribed to cDNA with qScript cDNA SuperMix (157031; Quanta Biosciences). PCR was conducted with PrecisionFAST qPCR Master Mix (FASR-LR-SY; Primerdesign Ltd, U.K.) with use of Applied Biosystems StepOnePlus Real-Time PCR System (Life Technologies). The expression levels of respective target genes were normalized to GAPDH, and relative gene expressions were calculated using standard $2^{-\Delta\Delta CT}$ method. Primers used in this study are listed in Table 1.

SDS-PAGE and Western Blotting

Cells or tissues were lysed on ice in radioimmunoprecipitation assay buffer containing 0.0037 mg/mL protease inhibitor (Roche), 1 mmol/L dithiothreitol (cat. no. D9779; Sigma-Aldrich), 1 mmol/L phenylmethylsulfonyl fluoride (P7626; Sigma-Aldrich), and 100 mmol/L phosphatase inhibitors (P0044 [for cell signaling experiments]; Sigma-Aldrich). Proteins were separated by 10% SDS-PAGE before being transferred onto an Immobilon-PSQ PVDF Membrane (ISEQ-00010; Merck Millipore). Blots were probed with LRG1 antibody (rabbit monoclonal, 13224-1-AP; Proteintech), phosphorylated (phospho-)Smad1/5 antibody (rabbit monoclonal, 9516; Cell Signaling Technology), anti-SMAD1+ SMAD5 antibody (mouse monoclonal, ab75273; Abcam), histone H3 (citrulline R2 + R8 + R17) antibody (rabbit polyclonal, ab5103; Abcam), histone H3 antibody (rabbit polyclonal, ab1791; Abcam), phospho-Akt antibody (rabbit monoclonal, 4060; Cell Signaling Technology), Akt antibody (rabbit monoclonal, 9272; Cell Signaling Technology), cyclin D1 antibody (rabbit monoclonal, 2922; Cell Signaling Technology), or GAPDH antibody (rabbit polyclonal, sc-25778; Santa Cruz Biotechnology), followed by horseradish peroxidase–conjugated secondary antibodies (Santa Cruz Biotechnology). Densitometry was performed by use of ImageJ software.

Molecular Biological Methods

Human LRG1 (NM_052972) carrying a 6xHis tag expression vector, pcDNA3.1-LRG1, was generated as previously

Table 1—qRT-PCR primer sequences

Gene	Forward primer sequence	Reverse primer sequence
Mouse		
Lrg1	5′-TGCACCTCTCGAGCAATCG-3′	5′-TGCAGGCGCTGTCTCCCGAGTT-3′
Gapdh	5′-AGGTCGGTGTGAACGGATTTG-3′	5′-TGTAGACCATGTAGTTGAGGTCA-3′
Human		
LRG1	5′-GTTGGAGACCTTGCCACCT-3′	5′-GCTTGTTGCCGTTCAGGA-3′
ICAM 1	5′-AGGGTAAGGTTCTTGCCCAC-3′	5′-TGATGGGCAGTCAACAGCTA-3′
VCAM 1	5′-GTCTCCAATCTGAGCAA-3′	5′-TGGGAAAAACAGAAAAGAGGTG −3′
P-selectin	5′-TGAGCACTGCTTGAAGAAAAAGC-3′	5′-CACGTATTCACATTCTGGCCC-3′
E-selectin	5′-TGTTTCCAAAACCCTGGAAG-3′	5′-AACTGGGATTTGCTGTGTCC-3′
GAPDH	5′-GGTCTCCTCTGAC TTCAACA-3′	5′-AGCCAAATTCGTTGTCATAC-3′

described (11). rhLRG1 protein was expressed in Freestyle 293 T cells (Invitrogen) and purified as previously described (11). siRNA oligonucleotides (cat. no. L-015179-01; Dharmacon) were used for LRG1 gene knockdown, while control siRNA (D-001810-10-20; Dharmacon) was used as a negative control. Transfection was performed using Lipofectamine 2000 (Invitrogen) for HaCaT cells and RNAiMAX (Invitrogen) for dHL-60 cells according to the manufacturer's protocol.

Flow Cytometry

Cell-surface CD11b and L-selectin were measured using flow cytometry. dHL-60 cells were treated with rhLRG1 (20 μg/mL) for 1 h, 6 h, or 24 h before being washed with flow buffer (0.1% FBS/PBS). Cells were then incubated with L-selectin antibody (mouse monoclonal, cat. no. sc-390756; Santa Cruz Biotechnology), followed by staining with Alexa Fluor 488 goat anti-mouse (IgG) secondary antibody (Thermo Fisher Scientific) and CD11b-phycoerythrin (130-113-235; Miltenyi Biotec) and fixation in 1% paraformaldehyde. Cell acquisition (10,000 cells per sample) was carried out on BD LSRFortessa X-20 (BD Biosciences) and analyzed with use of FlowJo software (BD).

Neutrophil Adhesion Assay

Lrg1-knockdown dHL-60 cells or dHL-60 cells treated with rhLRG1 (20 μg/mL) cells were labeled with CellTracker Green CMFDA Dye (Invitrogen) before being seeded onto the confluent HDMEC monolayer. In the case of *Lrg1*-knockdown dHL-60 cells, HDMECs were pretreated with tumor necrosis factor (TNF)α (50 ng/mL; PeproTech). Two hours later, nonadherent neutrophils were subsequently removed by washing with prewarmed PBS. Adherent neutrophils were imaged with the Eclipse Ti-E Inverted Research Microscope (Nikon Instruments, Tokyo, Japan) and quantified by measurement of the fluorescence intensity with Synergy H1 microplate reader (BioTek) at the wavelength of 492 nm/517 nm.

Proliferation Assay

HDMECs were cultured in EGM-2MV media (Lonza, Basel, Switzerland) until 30% confluent and starved in EBM-2 medium (Lonza) containing 0.2% FBS for 16 h before being treated with rhLRG1 (20 μg/mL) for 48 h. Cells were then fixed and stained with Ki67 antibody (rabbit polyclonal antibody, cat. no. ab15580; Abcam) for detection of proliferating cells and DAPI (Thermo Fisher Scientific) for staining cell nuclei. Images were taken with Eclipse Ti-E Inverted Research Microscope and analyzed with ImageJ. Proliferation rate was calculated as the percentage of $Ki67^+$ cells.

Transwell Migration Assay

HDMECs were pretreated with rhLRG1 for 24 h before being seeded onto rat tail collagen I (100 μg/mL; Corning)–coated Transwell Inserts (8 μm) (Corning). EBM2 medium containing 5% FBS served as a chemoattractant. After 5-h incubation, migrated cells were fixed and stained with DAPI (Thermo Fisher Scientific). Images were taken with Eclipse Ti-E Inverted Research Microscope and analyzed with Image J.

Matrigel Tube Formation Assay

Matrigel Growth Factor Reduced Basement Membrane Matrix (Corning) (60 μL) containing vehicle control or rhLRG1 (20 μg/mL) was added to each well of a 96-well plate and incubated for 30 min at 37°C for polymerization. HDMECs in 100 μL EBM-2 medium containing vehicle control or rhLRG1 (20 μg/mL) were seeded onto the polymerized Matrigel gel. HDMEC tube formation was imaged using phase-contrast mode on Eclipse Ti-E Inverted Research Microscope following overnight incubation, and tube formation was analyzed with ImageJ.

Trypan Blue Exclusion Assay

Transfected and rhLRG1 (2 μg/mL)–treated HaCaT cells were trypsinized and stained with Trypan blue before being counted with a hemocytometer under a phase-contrast microscope.

Scratch Wound Healing Assay

Confluent HaCaT cells were starved in DMEM medium containing 0.2% FBS (Thermo Fisher Scientific) for 24 h. A scratch was made to HaCaT cell monolayer with a sterile p200 pipette tip. The cells were washed and subsequently cultured in complete DMEM. Cells were imaged at 0 h and 24 h after scratching with Eclipse Ti-E Inverted Research Microscope 24 h after scratching. Images were analyzed with ImageJ.

SYTOX Green Assay

Primary mouse and human peripheral blood neutrophils were seeded onto each well of a 96-well black polystyrene microplate with a clear flat bottom (Corning). Cells were treated with 5 μmol/L calcium ionophore A23187 or rhLRG1 (100 μg/mL) for 4 h before incubation with the DNA dye SYTOX Green (1 μmol/L) (Invitrogen) for 15 min. NET formation was determined by measurement of the fluorescence intensity with Synergy H1 microplate reader (BioTek) at the wavelength of 504 nm/523 nm.

Induction of NETosis

Primary mouse neutrophils in RPMI-1640 medium containing 25 mmol/L HEPES were seeded onto each well of an eight-well chamber slide. Twenty minutes later, attached cells were incubated with 5 μmol/L calcium ionophore A23187 for 2 h before being fixed and stained with H3Cit antibody (1:100 dilution; Abcam) and DAPI (Thermo Fisher Scientific). Images were taken with Carl Zeiss LSM 710 confocal microscopy and analyzed with ImageJ.

Statistical Analysis

Data are represented as mean ± SEM. Statistical analyses were performed using unpaired, two-tailed Student *t* test

or one-way/two-way ANOVA followed by Tukey/Bonferroni post-test analysis using Prism 5 (GraphPad Software Inc.).

Data and Resource Availability

Complete data sets generated and analyzed during the current study are available from X.W. on request.

RESULTS

LRG1 Is Produced by Wound-Infiltrating Bone Marrow–Derived Cells Following Injury

To address the role of LRG1 in wound healing, we examined the expression of LRG1 in normal C56BL/6 mouse skin tissues by immunohistochemistry and revealed a very weak staining in the dermis (Fig. 1*A*). Western blot was used to evaluate LRG1 expression in wound tissues at various time points following injury (Fig. 1*B*). Our data showed that LRG1 was increased as early as 6 h post-injury and reached its highest level 24 h after wounding. LRG1 level then declined gradually and went back to basal level on day 5 following injury. It is worth noting that LRG1 expression in surrounding intact skin tissues remained low throughout the wound healing process (Supplementary Fig. 1).

Immunofluorescence staining was used to identify the source of LRG1 during wound healing. We found that $Lrg1^{+}$ cells were mainly present in the provisional matrix and were colocalized with $CD11b^{+}$ myeloid cells in day 1 wound tissues (Fig. 1*C*). Flow cytometry analysis revealed that LRG1 is expressed by $Ly6G^{+}/CD11b^{+}$ neutrophils, $Ly6C^{+}/CD11b^{+}$ monocytes, $Ly6C^{-}/F4/80^{+}/CD11b^{+}$ macrophages, and $Ly6C^{-}/F4/80^{+}/MHC\ II^{+}/CD11c^{+}/CD11b^{+}$ dendritic cells (Supplementary Fig. 2), all of which are bone marrow–derived cells. For confirmation of this observation, allogenic bone marrow transplantation (BMT) study was carried out in irradiated wild-type mice with use of BMCs from $Lrg1^{-/-}$ mice and wild-type littermate controls. Similar to what we observed in unirradiated C56BL/6 mice, quantitative real-time-PCR (qRT-PCR) showed that *Lrg1* transcript was significantly higher in day 1 wound tissues of wild-type mice transplanted with wild-type BMCs, whereas *Lrg1* was not induced in those that received $Lrg1^{-/-}$ BMCs (Fig. 1*D*). These data suggest that wound-infiltrating bone marrow–derived cells (BMDCs) serve as a major source of LRG1 during cutaneous wound healing.

LRG1 Is Critical for Timely Wound Closure

For elucidation of the functional role of LRG1 in cutaneous would healing, 4-mm full-thickness wounds were created on the dorsal skin of wild-type and $Lrg1^{-/-}$ mice. $Lrg1^{-/-}$ mice demonstrated a significant delay in wound closure as compared with wild-type controls in both excisional wound model and excisional wound splinting model

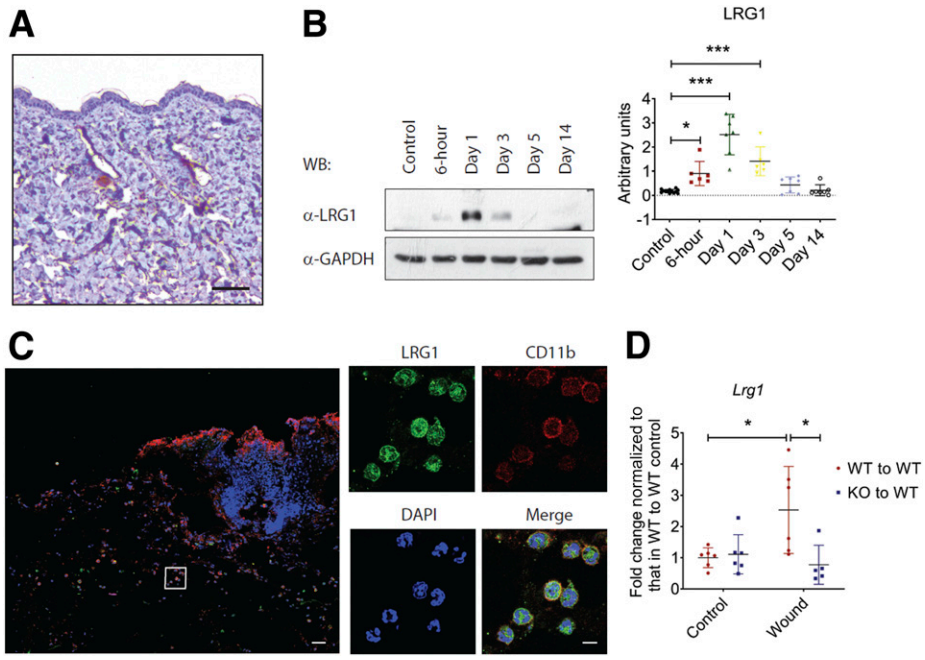

Figure 1—LRG1 is elevated in cutaneous wounds. *A*: Immunohistochemical detection of LRG1 (brown) showed low expression of LRG1 in normal mouse skin. Scale bar: 100 μm. *B*: Representative Western blot (left) and densitometry analysis (right) of wounds harvested at different time points. *C*: Immunofluorescence staining detecting LRG1 (green), CD11b (red), or DAPI (blue) in day 1 mouse wounds. Scale bars: 120 μm and 20 μm. *D*: qRT-PCR analysis of day 1 wounds demonstrated reduced *Lrg1* expression in irradiated wild-type mice with $Lrg1^{-/-}$ BMC transplantation in comparison with wild-type mice receiving wild-type BMCs. All images are representative; data are represented as mean (95% CI; *P*) of $n \geq 5$ mice per group. Significance was determined by one- or two-way ANOVA followed by Tukey multiple comparisons test. $^{*}P < 0.05$, $^{***}P < 0.001$. WB, Western blot; WT, wild type.

(Fig. 2*A* and Supplementary Fig. 3). As LRG1 is markedly induced at the inflammatory phase of wound healing, the number of wound-infiltrating immune cells was analyzed in the wound bed of wild-type and *Lrg1*$^{-/-}$ mice. Neutrophils are the first inflammatory cells to be recruited to the wound bed (26). After performing their functions, apoptotic neutrophils and tissue debris are cleared by macrophages, which eventually leads to the resolution of inflammation (27). Immunofluorescence staining showed a significant reduction in the number of wound-infiltrating MPO^{+} neutrophils (Fig. 2*B*) and F4/80^{+} macrophages (Fig. 2*C*) 1 day and 5 days post-injury, respectively. As BMDCs are major LRG1-producing cells, we next performed BMT between *Lrg1*$^{-/-}$ mice and wild-type controls. Mice subjected to irradiation were previously reported to show delayed wound repair (28). In this study, irradiated *Lrg1*$^{-/-}$ mice and wild-type control mice were intravenously transplanted with wild-type or *Lrg1*$^{-/-}$ BMCs, respectively (Fig. 2*D*). Wild-type mice transplanted with wild-type BMCs and *Lrg1*$^{-/-}$ mice transplanted with *Lrg1*$^{-/-}$ BMCs served as controls to exclude the impact of irradiation on wound healing. Consistent with what was observed in unirradiated control mice, wound closure was significantly delayed in *Lrg1*$^{-/-}$ recipients transplanted with *Lrg1*$^{-/-}$ BMCs as compared with that in wild-type recipients transplanted with wild-type BMCs. On the other

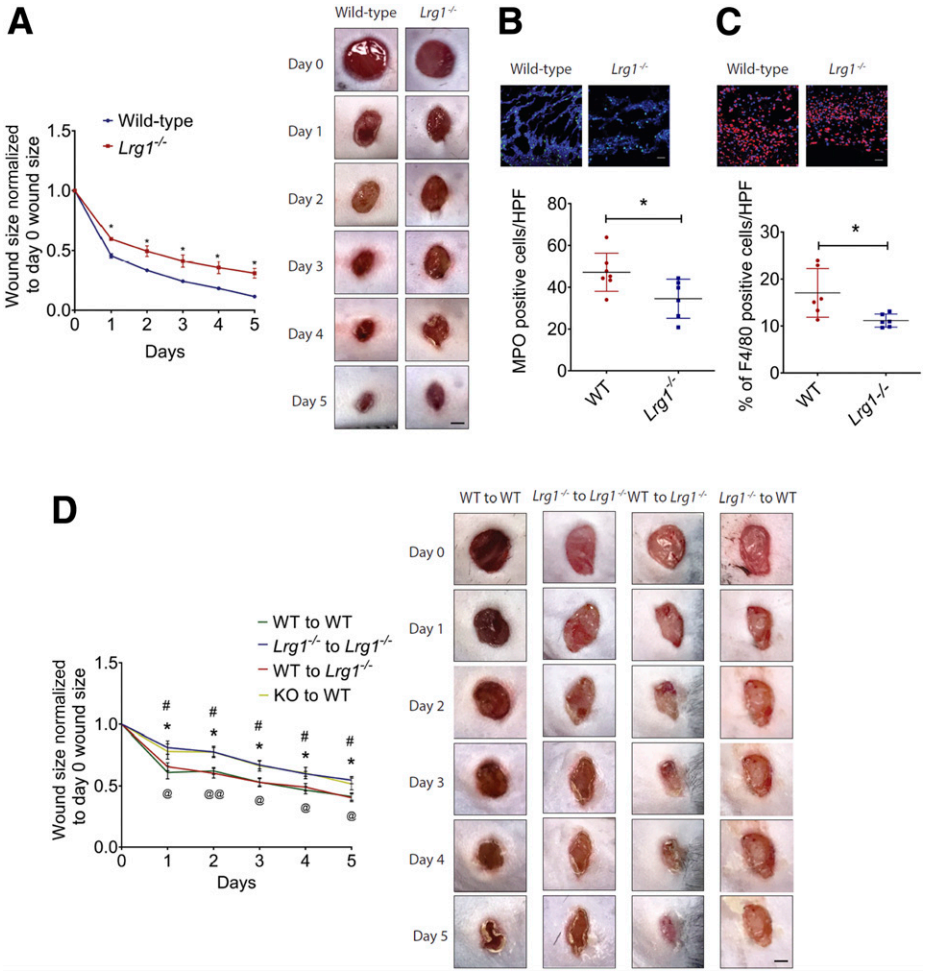

Figure 2—Absence of Lrg1 leads to delayed wound healing. *A*: Quantification (left) and representative images (right) of wound size in wild-type and *Lrg1*$^{-/-}$ mice revealed a delayed wound closure in the absence of Lrg1. *$P < 0.05$. Scale bar: 1 mm. *B*: Representative immunofluorescence staining of MPO (green) and DAPI (blue) (top) and quantification of the presentation of MOP^{+} cells (bottom) in day 1 wounds of wild-type and *Lrg1*$^{-/-}$ mice; 5–10 fields per wound were analyzed. *$P < 0.05$. Scale bar: 30 μm. *C*: Representative immunofluorescence staining of F4/80 (green) and DAPI (blue) (top) and quantification of F4/80^{+} cells (bottom) of day 5 mouse wounds of wild-type and *Lrg1*$^{-/-}$ mice; 5–10 fields per wound were analyzed. *$P < 0.05$. Scale bar: 30 μm. *D*: Quantification (left) and representative images (right) of wound size in irradiated wild-type (WT) mice receiving BMCs from wild-type mice (WT to WT), irradiated *Lrg1*$^{-/-}$ mice receiving BMCs from *Lrg1*$^{-/-}$ mice (*Lrg1*$^{-/-}$ to *Lrg1*$^{-/-}$), irradiated *Lrg1*$^{-/-}$ mice receiving BMCs from wild-type mice (WT to *Lrg1*$^{-/-}$), and irradiated wild-type mice receiving BMCs from *Lrg1*$^{-/-}$ mice (*Lrg1*$^{-/-}$ to WT). *$P < 0.05$: *Lrg1*$^{-/-}$ to *Lrg1*$^{-/-}$ vs. WT to WT; #$P < 0.05$: *Lrg1*$^{-/-}$ to WT vs. WT to WT; @$P < 0.05$, @@$P < 0.01$: WT to *Lrg1*$^{-/-}$ vs. *Lrg1*$^{-/-}$ to *Lrg1*$^{-/-}$. Scale bar: 1 mm. All images are representative; data are represented as mean (95% CI; *P*) of $n \geq 6$ mice per group. Significance was determined by unpaired, two-tailed Student *t* test between wild-type and *Lrg1*$^{-/-}$ or wound size at different time points.

hand, wound closure in wild-type recipients transplanted with *Lrg1*$^{-/-}$ BMCs was delayed substantially, whereas wild-type BMCs fully rescued the delayed wound healing in *Lrg1*$^{-/-}$ mice. Together, these data provide compelling evidence that LRG1-producing BMDCs are critical for timely wound closure.

LRG1 Promotes Neutrophil Adhesion via Inducing the Expression of L-Selectin

The ability of neutrophils to adhere to the endothelium is critical for their recruitment to the wound bed (29). To understand LRG1's role in neutrophil infiltration, we investigated the ability of dHL-60 cells to adhere to a HDMEC monolayer in the presence and absence of rhLRG1. Our study showed that rhLRG1 significantly promoted dHL-60 cell adhesion to the HDMEC monolayer (Fig. 3*A*). As dHL-60 cells express higher levels of LRG1 compared with other skin cells (Supplementary Fig. 4), we went on investigating the consequence of siRNA-mediated LRG1 knockdown in neutrophil function and demonstrated reduced responsiveness to TNFα-induced adhesion to HDMECs (Fig. 3*B*). L-selectin, a cell adhesion molecule expressed on neutrophils, serves as a master regulator of neutrophil adhesion (30). We next examined whether LRG1 exerts its function through mediating the expression of L-selectin on neutrophil-like dHL-60 cells. Indeed, immunoblots showed a significant increase in L-selectin expression in dHL-60 cells subjected to 24-h treatment with rhLRG1 (Fig. 3*C*). Consistent with this, flow cytometry revealed a marked increase of the median of fluorescence intensity in dHL-60 following rhLRG1 treatment (Fig. 3*D* and Supplementary Fig. 5). However, rhLRG1 did not affect the expression of endothelial adhesion molecules including ICAM-1, VCAM-1, P-selectin, and E-selectin (Supplementary Fig. 6). Together, these data show that LRG1 promotes neutrophil adhesion, at least partially, by regulating the expression of L-selectin on neutrophils.

LRG1 Promotes Epithelial Cell Proliferation and Epithelial-to-Mesenchymal Transition

Besides inflammation, reepithelialization is essential to prompt wound repair. It is achieved by orchestrated migration and proliferation of epithelial cells adjacent to the wound (31). H-E analysis revealed delayed reepithelialization in day 4 wounds of *Lrg1*$^{-/-}$ mice (Fig. 4*A*). Although the denuded surface is completely covered by newly formed epithelium 5 days following injury, the reconstituted epidermis is significantly thinner in *Lrg1*$^{-/-}$ mice as compared with that in wild-type controls (Fig. 4*B*). It was previously reported that exogenous LRG1 promotes keratinocyte migration (21). Similarly, we showed that LRG1-overexpressing HaCaT cells migrated much faster as compared with control plasmid transfected cells, whereas the migration ability of the LRG1 siRNA-treated HaCaT was significantly compromised (Fig. 4*C*). Activation of the partial epithelial-to-mesenchymal transition (EMT) has been reported to drive keratinocyte migration (32). Our study demonstrated that rhLRG1 was able to cause a significant induction of key EMT markers, such as fibronectin (FN1) and N-cadherin (N-Cad) (Fig. 4*D*). To define LRG1's role in reepithelialization

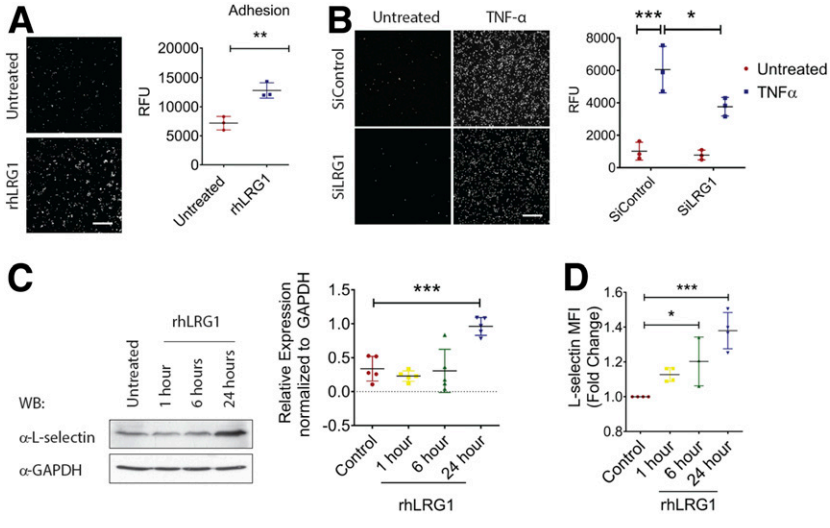

Figure 3—LRG1 mediates neutrophil adhesion. *A*: Representative images (left) and quantification (right) of neutrophil adhesion assay demonstrated rhLRG1 induced dH60 cell (labeled with CMFDA dye) adhesion to HDMECs. Scale bar: 200 μm. *B*: Representative images (left) and quantification (right) of TNFα-induced neutrophil adhesion by use of hHL-60 cells (labeled with CMFDA dye) subjected to siRNA-mediated LRG1 knockdown. Scale bar: 200 μm. *C*: Representative Western blot (left) and densitometry analysis (right) of L-selectin and GAPDH in rhLRG1-treated dHL-60 cells at different time points. *D*: Quantification of flow cytometry demonstrated an increase in L-selectin^{High} population following rhLRG1treatment. All images are representative; data are presented as the mean (95% CI; *P*) of $n \geq 3$ independent experiments per group. Significance was determined by one- or two-way ANOVA followed by Tukey multiple comparisons test or unpaired, two-tailed Student *t* test. $^{*}P < 0.05$, $^{**}P < 0.01$, $^{***}P < 0.001$. WB, Western blot.

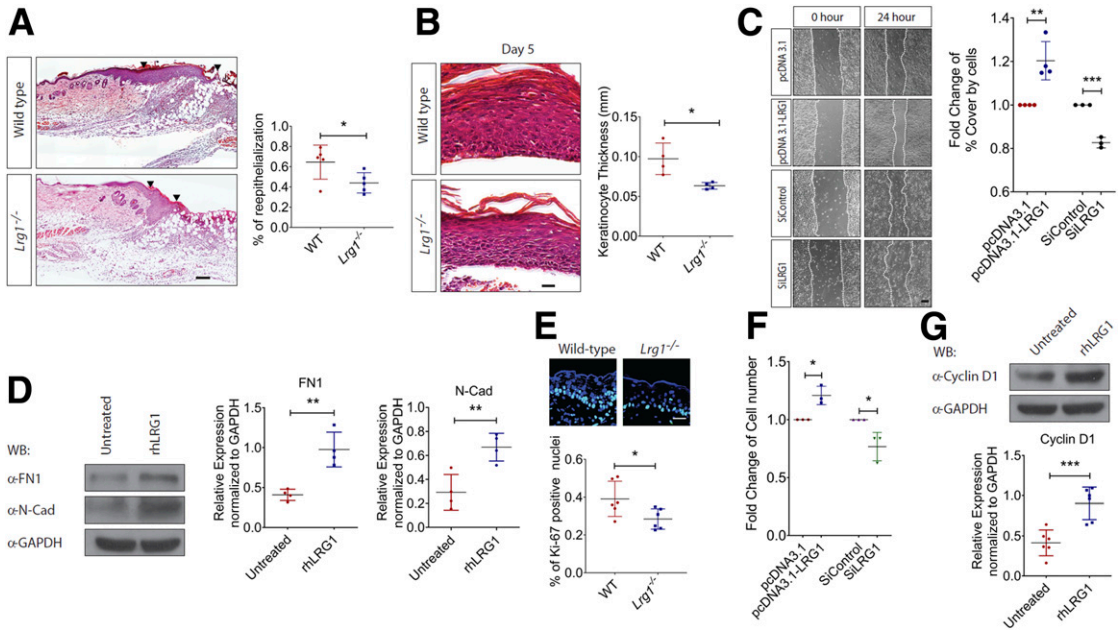

Figure 4—LRG1 regulates reepithelialization during wound healing. *A*: Representative H-E staining (left) and quantification of reepithelialization (right) of day 4 wounds of wild-type and *Lrg1*$^{-/-}$ mice. Scale bar: 125 μm. *B*: Representative H-E staining (left) and quantification of epithelium thickness (right) of day 5 wounds of wild-type and *Lrg1*$^{-/-}$ mice. Scale bar: 25 μm. *C*: Representative images (left) and quantification of wound gap (right) in scratch wound healing assay. Scale bar: 100 μm. *D*: Representative Western blot (left) and densitometry analysis (right) of FN1, N-cad, and GAPDH in rhLRG1-treated HaCaT cells. *E*: Representative immunofluorescence staining (top) and quantification (bottom) of Ki67 (red) and DAPI (blue) in day 3 wounds. Scale bar: 30 μm. *F*: Quantification of viable HaCaT cells in Trypan blue exclusion assay (*G*). Representative Western blot (top) and densitometry analysis (bottom) of cyclin D1 and GAPDH in rhLRG1-treated HaCaT cells. All images are representative, and data are represented as mean (95% CI; *P*) of $n \geq 5$ mice or $n \geq 3$ independent experiments per treatment group. Significance was determined by unpaired, two-tailed Student *t* test. $^{*}P < 0.05$, $^{**}P < 0.01$, $^{***}P < 0.001$. WB, Western blot.

further, we examined the keratinocyte proliferation as indicated by immunofluorescence staining with Ki67 in day 3 wounds of *Lrg1*$^{-/-}$ and wild-type control mice. Our study revealed a substantial reduction in the percentage of Ki67^{+} keratinocytes at the wound edge of *Lrg1*$^{-/-}$ mice (Fig. 4*E*). Consistent with this observation, the number of viable LRG1-overexpressing HaCaT cells was significantly higher than control cells, and HaCaT cells subjected to siRNA-mediated LRG1 knockdown showed reduced viability compared with control siRNA-treated HaCaT (Fig. 4*F*). This observation was supported by a marked increase in cell proliferation marker cyclin D1 in rhLRG1-treated HaCaT (Fig. 4*G*). Together, these data suggest that LRG1 facilitates reepithelialization by promoting keratinocyte proliferation and migration.

LRG1 Modulates Dermal Angiogenesis

Our previous study demonstrated an essential role of LRG1 in pathological neovascularization in the eye (11), and angiogenesis is required for the formation of granulation tissue during wound healing (1). To understand LRG1's role in dermal angiogenesis during wound healing, day 7 wound tissues were subjected to immunofluorescence staining with an endothelial cell (EC)-specific marker, CD31. Although the total vessel area in the distal part of the skin remained unchanged (Supplementary Fig. 7), there was a significant reduction in total vessel area in the wound bed of *Lrg1*$^{-/-}$ mice (Fig. 5*A*). In line with the observations in macrovascular human umbilical vein endothelial cells (HUVECs) (11), rhLRG1 was able to induce HDMEC proliferation as visualized by Ki67 staining (Fig. 5*B*) and the ability of HDMECs to form tube-like structure in Matrigel (Fig. 5*C*). We also showed increased motility of rhLRG1-treated HDMECs (Fig. 5*D*). Mechanistically, we found that rhLRG1 significantly stimulated the phosphorylation of proangiogenic Smad1/5 in HDMECs, and blocking of TGFβ type I receptor activin-like kinase 1 (ALK1) and activin-like kinase 5 (ALK5) completely abrogated this activation (Fig. 5*E*). These data demonstrate an ALK1/5-dependent proangiogenic role of LRG1 in wound healing.

LRG1 Is Highly Induced in Diabetic Mice and in Humans With Diabetes

Having established an important role for LRG1 in physiological wound healing, we next examined the association between LRG1 and chronic wound healing in mice and humans with diabetes. ELISA analysis revealed a significantly higher LRG1 level in the serum of DFU patients as compared with that in venous ulcer patients (Fig. 6*A*). Consistent with this, we showed that LRG1 expression in ulcer tissues of DFU patients was also significantly higher than that from venous ulcer patients (Fig. 6*B*). To support this observation, we analyzed wound tissues collected from C57BL/6 mice subjected to STZ-induced diabetes for the expression of LRG1. As observed in DFU patients, LRG1

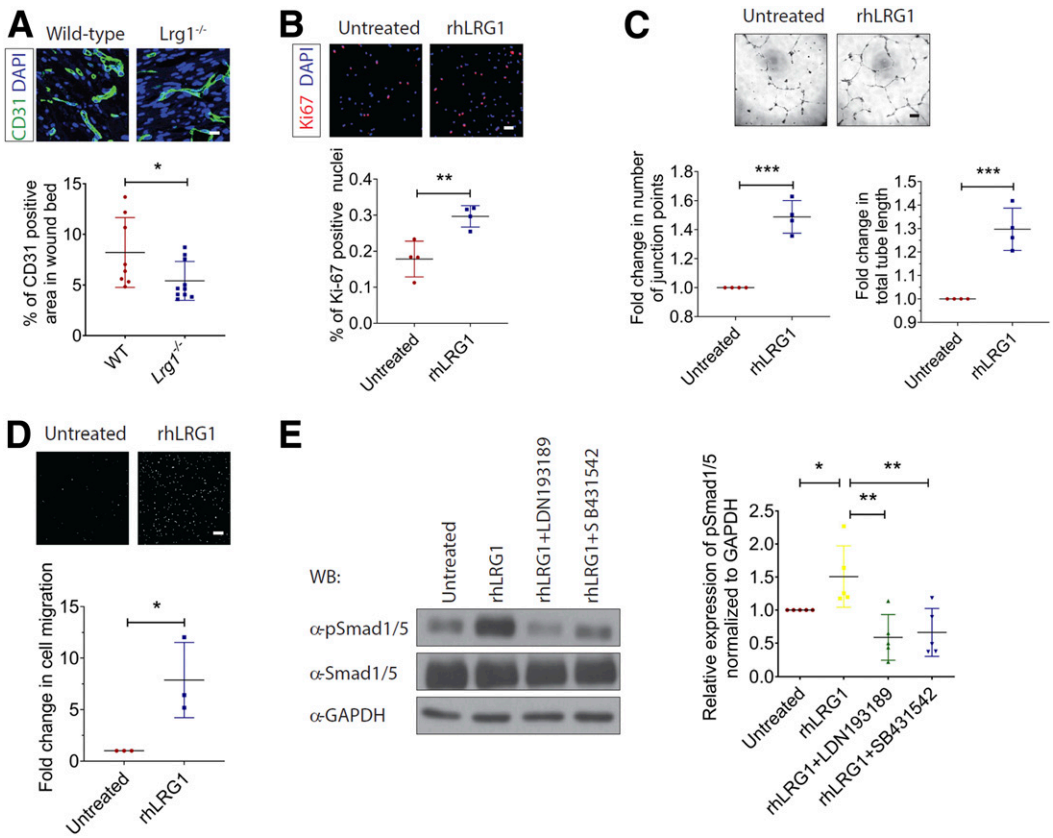

Figure 5—LRG1 modulates wound angiogenesis during wound healing. *A*: Representative immunofluorescence staining of CD31 (green) and DAPI (blue) (top) and quantification of vessel density (bottom) in day 7 wounds of wild-type and *Lrg1*$^{-/-}$ mice. Scale bar: 15 μm. *B*: Representative images of immunofluorescence staining detecting Ki67 (red) and DAPI (blue) (top) and quantification of percentage of Ki67^{+} cells (bottom) in HDMECs. Scale bar: 50 μm. *C*: Representative images (top) and quantification (bottom) of Matrigel tube formation. Scale bar: 125 μm. *D*: Representative images (top) and quantification (bottom) of Transwell migration assay. Scale bar: 100 μm. *E*: Representative Western blot (left) and densitometry analysis (right) of endothelial TGFβ-Smad1/5 signaling in HDMECs treated with rhLRG1 in the absence and presence of ALK1 inhibitor (LDN193189) or ALK5 inhibitor (SB431542). All images are representative, and data are represented as mean (95% CI; *P*) of $n \geq 6$ mice or $n \geq 3$ independent experiments per group. Significance was determined by unpaired, two-tailed Student *t* test. $^{*}P < 0.05$, $^{**}P < 0.01$, $^{***}P < 0.001$. WB, Western blot.

levels were significantly higher in wounds of diabetic mice (Fig. 6*C*). Consistently, qRT-PCR analysis revealed a sustained high expression of *Lrg1* transcript in the wound tissue of diabetic mice throughout the wound healing process (Fig. 6*D*). Wound closure was significantly impaired in diabetic mice as compared with that in nondiabetic control (Fig. 6*E*). These data show that in the skin, LRG1 expression is further increased in both humans and mice with diabetes.

Deletion of the Lrg1 Gene Was Beneficial to Impaired Wound Healing in Diabetes

As our data thus far have demonstrated an elevated *Lrg1* transcript level in wounds of both mice and humans with diabetes, we investigated whether wound closure in mice with STZ-induced diabetes is affected in the absence of *Lrg1*. Although STZ treatment led to a significant weight loss, there was no difference in body weight between STZ-treated wild-type and *Lrg1*$^{-/-}$ mice (Supplementary Fig. 8). Unlike what was observed in normoglycemic mice, mice with genetic deletion of *Lrg1* were protected from the diabetes-induced delay in would closure (Fig. 7*A*). Recent studies highlighted the influence of diabetes on NET formation (8). Considering the role of LRG1 in neutrophil functions and its upregulation at the inflammatory phase of wound healing, we next studied whether LRG1 affects NETosis in mice subjected to STZ-induced diabetes. Western blot analysis showed a significant reduction in the expression of a NET marker, H3Cit, in day 3 wounds of diabetic *Lrg1*$^{-/-}$ mice (Fig. 7*B*). For confirmation of this observation, bone marrow–derived neutrophils were isolated from wild-type and *Lrg1*$^{-/-}$ mice and subjected to calcium ionophore–induced NETosis. Consistent with the earlier observation, *Lrg1*$^{-/-}$ neutrophils were resistant to calcium ionophore–induced expression of H3Cit (Fig. 7*C*). Similarly, immunofluorescence staining showed that calcium ionophore–induced NETs, as indicated by the presence of H3Cit^{+} neutrophils, were significantly reduced in *Lrg1*-deficient neutrophils (Fig. 7*D*). We also showed that *Lrg1*-deficient neutrophils formed fewer NETs in comparison

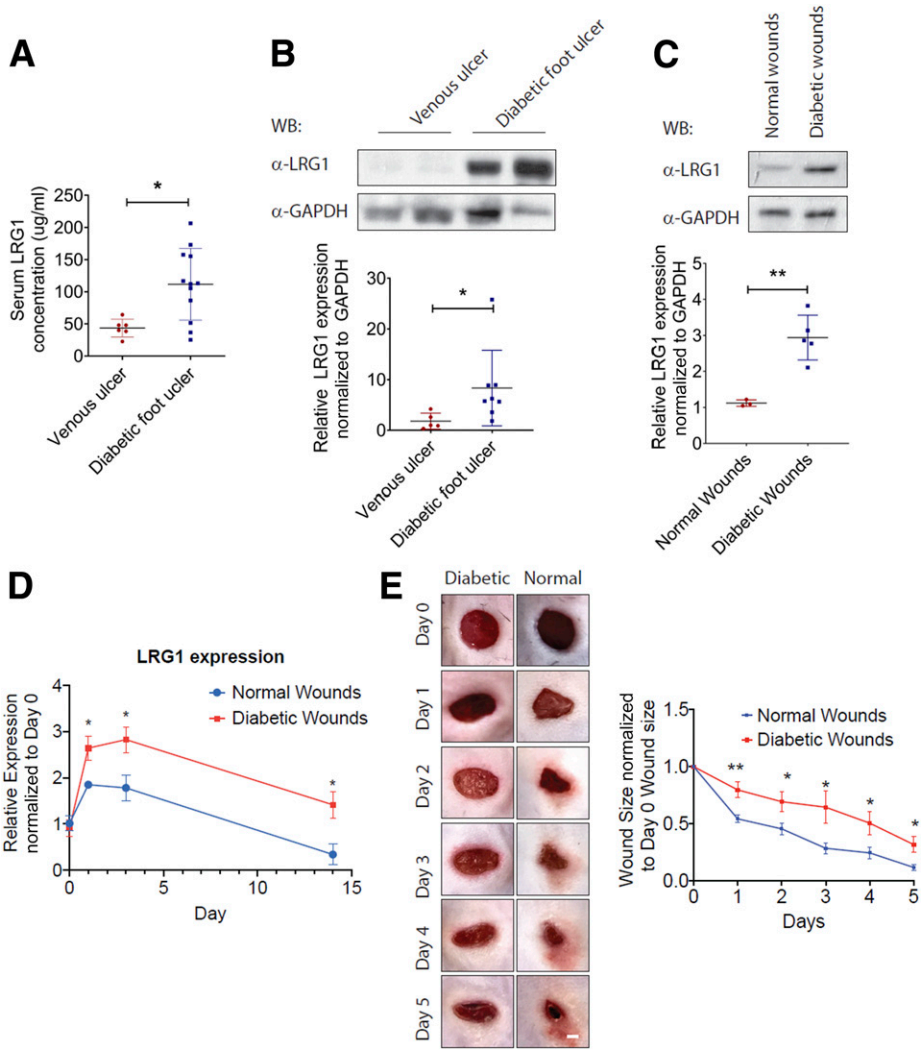

Figure 6—Elevated LRG1 expression is observed in diabetic humans and mice. *A*: ELISA analysis of LRG1 in serum from venous ulcer patients and DFU patients. *B*: Representative Western blot (top) and densitometry analysis (bottom) of LRG1 and GAPDH in human patients with venous ulcer and DFU. *C*: Representative Western blot (top) and densitometry analysis (bottom) of LRG1 and GAPDH in normal and diabetic wounds of C57BL/6 mice. *D*: qRT-PCR analysis of normal and diabetic wounds of C57BL/6 mice. *E*: Representative images (left) and quantification (right) of wound size revealed a delayed wound closure in C57BL/6 mice with STZ-induced diabetes. Scale bar: 1 mm. All images are representative, and data are represented as mean (95% CI; *P*) of $n \geq 6$ patients or mice per group. Significance was determined by unpaired, two-tailed Student *t* test. $^{*}P < 0.05$, $^{**}P < 0.01$. WB, Western blot.

with their wild-type counterparts upon calcium ionophore treatments (Fig. 7*E*). Complementing this observation, SYTOX Green assay showed that LRG1 supplementation significantly induced the formations of NETs in human peripheral blood neutrophils (Fig. 7*F*). Consistently, immunoblots demonstrated that rhLRG1 significantly induced citrullination of histone H3 in dHL-60 cells (Fig. 7*G*). Activation of Akt pathway was reported to mediate calcium ionophore–induced NETosis (33). We further showed that LRG1 was able to induce the phosphorylation of Akt in dHL-60 cells and the LRG1-induced expression of H3Cit and Akt phosphorylation were completely abolished in the presence of an allosteric Akt inhibitor, MK2206 (Fig. 7*G*). LRG1 was previously reported to signal through TGFβ type I receptor activin-like kinase 5 (ALK5) in non-ECs (34). For elucidation of whether LRG1-induced NETosis and Akt activation are dependent on ALK5, ALK5 was inhibited by SB431542, resulting in a complete abrogation of LRG1-induced phosphorylation of Akt and H3Cit (Fig. 7*H*). Together, our data demonstrate an important role of LRG1 in diabetic wounds and that LRG1 exerts its function through mediating NETosis in a TGFβ/ALK5/Akt-dependent manner.

DISCUSSION

Impaired wound healing and subsequent formation of foot ulcers is one of the most common complications found in patients with diabetes (2). Considering the important role of inflammation in DFU pathophysiology, multiple anti-inflammatory drugs have been developed but have shown limited success (10). LRG1 is a multifunctional protein

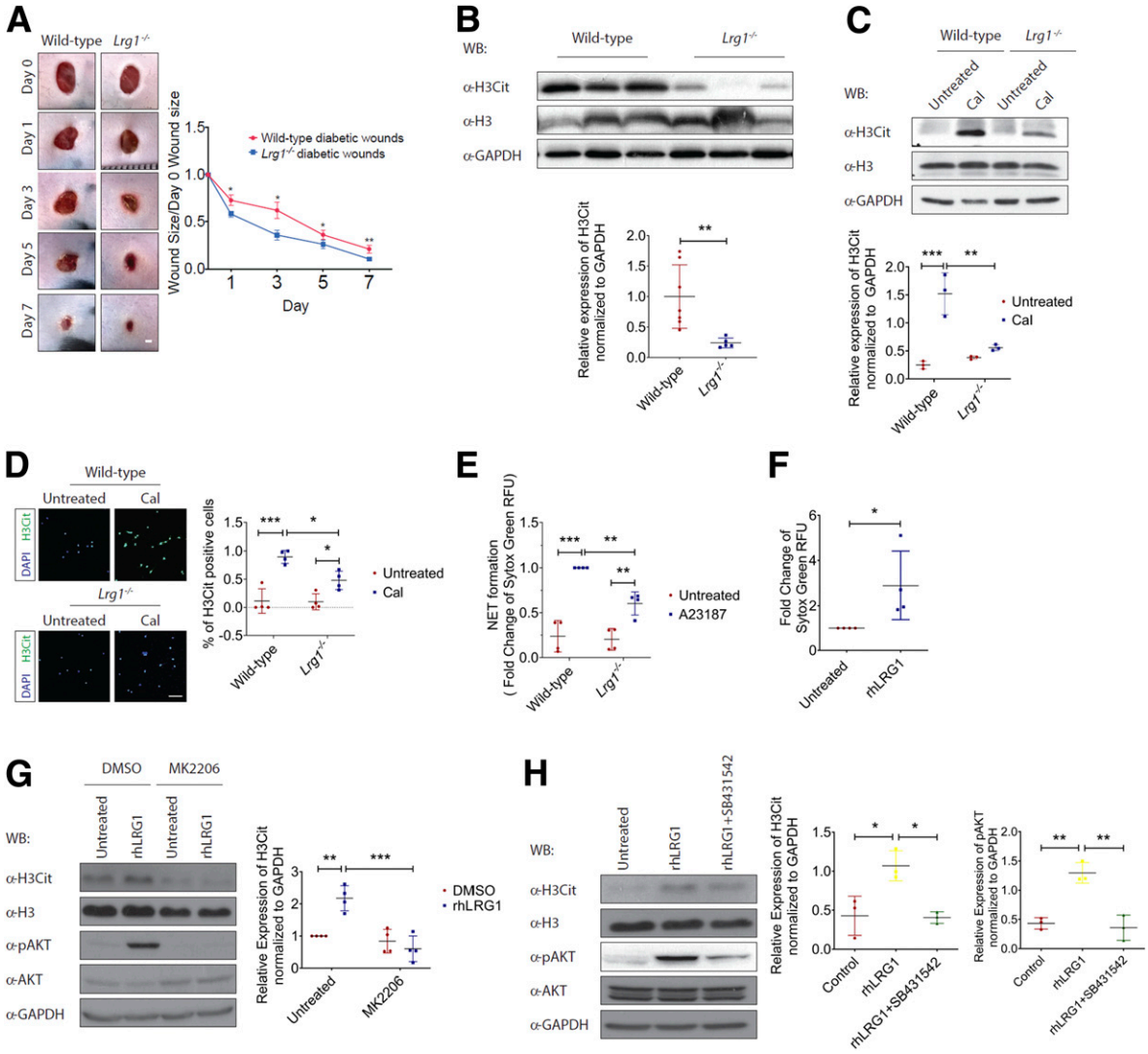

Figure 7— LRG1 mediates NETosis. *A*: Representative images (left) and quantification (right) of wound size in wild-type and *Lrg1*$^{-/-}$ mice with STZ-induced diabetes. Scale bar: 1 mm. *B*: Representative Western blot (top) and densitometry analysis (bottom) of H3Cit, histone H3 (H3), and GAPDH in day 3 wounds from wild-type and *Lrg1*$^{-/-}$ mice with STZ-induced diabetes. *C*: Representative Western blot (top) and densitometry analysis (bottom) of H3Cit, H3, and GAPDH in calcium ionophore–treated wild-type and *Lrg1*$^{-/-}$ neutrophils. *D*: Representative immunofluorescence staining detecting H3Cit (green) and DAPI (blue) (left) and quantification of percentage of H3Cit^{+} cells (right) in calcium ionophore–treated wild-type and *Lrg1*$^{-/-}$ neutrophils. Scale bar: 80 μm. *E*: SYTOX Green assay on calcium ionophore–treated wild-type and *Lrg1*$^{-/-}$ neutrophils. *F*: SYTOX Green assay on calcium ionophore–treated dHL-60 cells. *G*: Representative Western blot (left) and densitometry analysis (right) of H3Cit, H3, AKT, phospho-AKT (pAKT), and GAPDH in rhLRG1- and/or MK2206-treated dHL-60 cells. *H*: Representative Western blot (left) and densitometry analysis (right) of H3Cit, H3, AKT, phospho-AKT, and GAPDH in rhLRG1 with or without SB431542-treated dHL-60 cells. All images are representative, and data are represented as mean (95% CI; *P*) of $n \geq 5$ mice or $n \geq 3$ independent experiments per group. Significance was determined by one- or two-way ANOVA followed by Tukey multiple comparisons test or unpaired, two-tailed Student *t* test. $^{*}P < 0.05$, $^{**}P < 0.01$, $^{***}P < 0.001$. Cal, calcium ionophore; WB, Western blot.

that was previously linked to neutrophil activation (35), EMT (16), and angiogenesis (11), all of which are essential for effective wound closure. Here, we investigated the role of LRG1 in both physiological and pathological cutaneous wound healing.

Overwhelming evidence indicated the association between LRG1 and various inflammatory and autoimmune conditions (12–14). Infiltrating myeloid cells have been reported to act as the key source of LRG1 in psoriatic skin lesions (13) and remodeling myocardium following infarction (36). In line with these observations, our study revealed that LRG1 is predominantly produced by the wound-infiltrating CD11b^{+} myeloid cells. Neutrophils are among the first inflammatory cells to reach the wound bed following injury. Both impaired neutrophil function and hyperactive neutrophils have been reported to compromise wound healing (26). Despite being induced during early neutrophil differentiation (37), the role of LRG1 in neutrophil function remains to be elucidated. Our study showed that LRG1 promotes neutrophil adhesion, likely by inducing

the expression of neutrophil adhesion molecule, L-selectin. Consistent with this observation, the number of wound-infiltrating neutrophils was significantly reduced in the wound bed of *Lrg1*$^{-/-}$ mice. We further showed that wild-type recipients transplanted with *Lrg1*$^{-/-}$ BMCs showed a significant delay in wound closure as compared with wild-type recipients receiving wild-type BMCs. On the other hand, wild-type BMCs were sufficient to rescue the delayed wound closure in *Lrg1*$^{-/-}$ recipients. These data support the important role of BMDC-derived LRG1 in wound healing.

Reepithelialization plays an indispensable role in wound healing, and it is driven by the proliferation and migration of keratinocytes at the wound edge (31). A previous study using exogenous LRG1 showed that LRG1 does not affect keratinocyte proliferation as demonstrated by EdU^{+} staining (21). Here, we showed reduced number of proliferating keratinocytes as indicated by Ki67 staining at the wound edge of *Lrg1*-deficient mice. The discrepancy between the two studies is likely due to the use of different cellular markers for proliferating cell detection. Ki67 is a broad cell proliferation marker that is expressed throughout the active cell cycle (G1, S, G2, and M phases) (38), whereas EdU is only incorporated in nascent DNA during the S phase (39). Therefore, EdU may provide partial information regarding the extent of cell proliferation. Supporting LRG1's role in keratinocyte proliferation, plasmid-mediated LRG1 overexpression and siRNA-mediated LRG1 knockdown treatment significantly affect the viability of keratinocytes in vitro. We also demonstrated a promoting role of LRG1 in the expression of cell-cycle marker cyclin D1. These results are in line with previous studies that LRG1 increases proliferation of different epithelial-derived cancer cells, such as colorectal cancer cells (40), pancreatic ductal adenocarcinoma (17), non-small-cell lung cancer cells (41), and gastric cancer cells (15). Consistent with the previous report (21), we showed that LRG1 overexpression and knockdown affect keratinocyte migration. To acquire migratory capacity, quiescent epithelial cells undergo phenotypic changes to gain mesenchymal characteristics (42). Our study discovered that rhLRG1 induces the expression of EMT markers, which is consistent with the promoting effect of LRG1 in EMT and colorectal cancer metastasis (16).

The increased metabolic demand of repairing triggers angiogenesis, and failure in forming functional new vessel leads to delayed wound closure (43). Although LRG1 has previously been implicated in ocular (11) and tumor (16) angiogenesis, its role in normal blood vessel formation during wound healing was largely unknown. In this study, we observed reduced blood vessel density in the wound bed of *Lrg1*$^{-/-}$ mice. We further showed that LRG1 promotes angiogenesis by mediating HDMEC proliferation, migration, and the ability to form tube-like structures. Unlike what was observed in HUVECs (11), both ALK1 and ALK5 are required for LRG1-induced Smad1/5/8 phosphorylation in HDMECs, which is not surprising, as ALK5 kinase activity is necessary for optimal TGFβ/ALK1 action (44).

Our study showed elevated LRG1 levels in serum and wound tissues of human patients with DFU and diabetic mice, which could be explained, at least partially, by the increased infiltration of immune cells, including neutrophils and macrophages, in diabetic wounds (45). While neutrophils are beneficial to normal wound repair, excessive neutrophil infiltration and NET formation are critical culprits in chronic inflammation and delayed wound closure in diabetes (8). Mechanistically, NETosis could be triggered in a NADPH oxidase (NOX)-dependent and -independent manner (33). Our study showed that there was a reduced NETosis in *Lrg1*$^{-/-}$ mice and *Lrg1*$^{-/-}$ neutrophils are resistant to calcium ionophore–induced NOX-independent NETosis. Akt is essential for NOX-independent NETosis (33). Furthermore, we demonstrated that LRG1-mediated NET formation is dependent on activation of the Akt pathway through TGFβ type I receptor ALK5, which is in agreement with LRG1-mediated TGFβ signaling in ECs (11), fibroblasts (34), glioma cells (46), and T-helper 17 cells (47). We further demonstrated that *Lrg1*$^{-/-}$ mice are resistant to diabetes-induced delay in wound closure, especially during the inflammatory phase, which is likely due to its role in NETosis. It is worth highlighting that global *Lrg1*$^{-/-}$ mice were used in this study, whereas prompt wound healing is achieved by collaborative interactions between multiple types of cells present in the wound microenvironment (1). Our BMT and in vitro experiments provided a direct evidence of BMDC-derived LRG1 on the behavior of other types of skin cells, However, this would not exclude the possible impacts of EC and keratinocyte-derived LRG1 on inflammation, reepithelialization, and angiogenesis during wound closure. To address these questions, we are now generating cell-specific knockout mice.

In conclusion, we define here a complex but critical role of LRG1 in normal and diabetic wound healing. *Lrg1* deficiency leads to a significant delay in normal wound healing as a consequence of impaired inflammation, reepithelialization, and angiogenesis. On the other hand, there is a reduced NETosis in diabetic mice with ablation of *Lrg1*, which protects *Lrg1*$^{-/-}$ from the diabetes-induced delay in wound healing. Targeting LRG1 may represent an attractive strategy to suppress excessive NETosis, therefore accelerating wound closure in patients with diabetes.

Acknowledgments. The authors thank David Becker, Lee Kong Chian School of Medicine, for advice on histology analysis.

Funding. This work was supported by Singapore Biomedical Research Council SPF grant (SIPRAD) to X.W. and W.H. and Singapore National Medical Research Council DYNAMO NMRC/OFLCG/001/2017 and TAPP NMRC/OFLCG/004/2018 to X.W. Singapore Study of Macroangiopathy and Micro-vascular Reactivity in Type 2 Diabetes (SMART2D) is supported by the Singapore Ministry of Health's National Medical Research Council under its Clinician Scientist Individual Research Grant (CS-IRG) (MOH-000066).

Duality of Interest. No potential conflicts of interest relevant to this article were reported.

Author Contributions. C.L. designed the study, performed experiments, analyzed data, and wrote the manuscript. M.H.Y.T. and S.L.T.P. designed and

performed experiments and discussed data. M.L.L. and H.M.T. performed experiments. H.W.H., C.R., S.E.M., J.G., and S.T. contributed to discussion and reviewed and edited the manuscript. W.H. secured funding, conceived the project, contributed to discussion, and reviewed and edited the manuscript. X.W. secured funding, conceived the project, designed the study, and wrote the manuscript. X.W. is the guarantor of this work and, as such, had full access to all the data in the study and takes responsibility for the integrity of the data and the accuracy of the data analysis.

Prior Presentation. Parts of this study were presented in the abstract form at the 3rd Singapore International Conference on Skin Research, Singapore, 21 March 2018.

References

1. Gurtner GC, Werner S, Barrandon Y, Longaker MT. Wound repair and regeneration. Nature 2008;453:314–321
2. Armstrong DG, Boulton AJM, Bus SA. Diabetic foot ulcers and their recurrence. N Engl J Med 2017;376:2367–2375
3. Morbach S, Furchert H, Gröblinghoff U, et al. Long-term prognosis of diabetic foot patients and their limbs: amputation and death over the course of a decade. Diabetes Care 2012;35:2021–2027
4. Gregg EW, Li Y, Wang J, et al. Changes in diabetes-related complications in the United States, 1990-2010. N Engl J Med 2014;370:1514–1523
5. Wild S, Roglic G, Green A, Sicree R, King H. Global prevalence of diabetes: estimates for the year 2000 and projections for 2030. Diabetes Care 2004;27:1047–1053
6. Falanga V. Wound healing and its impairment in the diabetic foot. Lancet 2005;366:1736–1743
7. Diegelmann RF, Evans MC. Wound healing: an overview of acute, fibrotic and delayed healing. Front Biosci 2004;9:283–289
8. Wong SL, Demers M, Martinod K, et al. Diabetes primes neutrophils to undergo NETosis, which impairs wound healing. Nat Med 2015;21:815–819
9. Rosique RG, Rosique MJ, Farina Junior JA. Curbing inflammation in skin wound healing: a review. Int J Inflamm 2015;2015:316235
10. Patel S, Srivastava S, Singh MR, Singh D. Mechanistic insight into diabetic wounds: pathogenesis, molecular targets and treatment strategies to pace wound healing. Biomed Pharmacother 2019;112:108615
11. Wang X, Abraham S, McKenzie JAG, et al. LRG1 promotes angiogenesis by modulating endothelial TGF-β signalling. Nature 2013;499:306–311
12. Shimizu M, Inoue N, Mizuta M, Nakagishi Y, Yachie A. Serum leucine-rich α2-Glycoprotein as a biomarker for monitoring disease activity in patients with systemic juvenile idiopathic arthritis. J Immunol Res 2019;2019:3140204
13. Nakajima H, Serada S, Fujimoto M, Naka T, Sano S. Leucine-rich α-2 glycoprotein is an innovative biomarker for psoriasis. J Dermatol Sci 2017;86:170–174
14. Shinzaki S, Matsuoka K, Iijima H, et al. Leucine-rich alpha-2 glycoprotein is a serum biomarker of mucosal healing in ulcerative colitis. J Crohn's Colitis 2017;11:84–91
15. Yamamoto M, Takahashi T, Serada S, et al. Overexpression of leucine-rich α2-glycoprotein-1 is a prognostic marker and enhances tumor migration in gastric cancer. Cancer Sci 2017;108:2052–2060
16. Zhang J, Zhu L, Fang J, Ge Z, Li X. LRG1 modulates epithelial-mesenchymal transition and angiogenesis in colorectal cancer via HIF-1α activation. J Exp Clin Cancer Res 2016;35:29
17. Xie Z-B, Zhang Y-F, Jin C, Mao Y-S, Fu D-L. LRG-1 promotes pancreatic cancer growth and metastasis via modulation of the EGFR/p38 signaling. J Exp Clin Cancer Res 2019;38:75
18. Schäfer M, Werner S. Cancer as an overhealing wound: an old hypothesis revisited. Nat Rev Mol Cell Biol 2008;9:628–638
19. Pek SL, Tavintharan S, Wang X, et al. Elevation of a novel angiogenic factor, leucine-rich-α2-glycoprotein (LRG1), is associated with arterial stiffness, endothelial dysfunction, and peripheral arterial disease in patients with type 2 diabetes. J Clin Endocrinol Metab 2015;100:1586–1593
20. Pourghaderi P, Yuquimpo K, Sukpraprut-Braaten S, Waggoner D. Retrospective clinical study of lower extremity amputation in patients with diabetes mellitus and peripheral arterial disease: predictors of postoperative outcomes. J Am Coll Surg 2017;225:S144
21. Gao Y, Xie Z, Ho C, et al. LRG1 promotes keratinocyte migration and wound repair through regulation of HIF-1α stability. J Invest Dermatol 2020;140:455–464.e8
22. Kayal RA, Tsatsas D, Bauer MA, et al. Diminished bone formation during diabetic fracture healing is related to the premature resorption of cartilage associated with increased osteoclast activity. J Bone Miner Res 2007;22:560–568
23. Wang X, Ge J, Tredget EE, Wu Y. The mouse excisional wound splinting model, including applications for stem cell transplantation. Nat Protoc 2013;8:302–309
24. Kuhns DB, Priel DAL, Chu J, Zarember KA. Isolation and functional analysis of human neutrophils. Curr Protoc Immunol 2015;111:7.23.1–7.23.16
25. Mócsai A, Zhang H, Jakus Z, Kitaura J, Kawakami T, Lowell CA. G-protein-coupled receptor signaling in Syk-deficient neutrophils and mast cells. Blood 2003;101:4155–4163
26. Wang J. Neutrophils in tissue injury and repair. Cell Tissue Res 2018;371:531–539
27. Koh TJ, DiPietro LA. Inflammation and wound healing: the role of the macrophage. Expert Rev Mol Med 2011;13:e23
28. Rodriguez-Menocal L, Shareef S, Salgado M, Shabbir A, Van Badiavas E. Role of whole bone marrow, whole bone marrow cultured cells, and mesenchymal stem cells in chronic wound healing. Stem Cell Res Ther 2015;6:24
29. Muller WA. Getting leukocytes to the site of inflammation. Vet Pathol 2013;50:7–22
30. Nagaoka T, Kaburagi Y, Hamaguchi Y, et al. Delayed wound healing in the absence of intercellular adhesion molecule-1 or L-selectin expression. Am J Pathol 2000;157:237–247
31. Pastar I, Stojadinovic O, Yin NC, et al. Epithelialization in wound healing: a comprehensive Review. Adv Wound Care (New Rochelle) 2014;3:445–464
32. Stone RC, Pastar I, Ojeh N, et al. Epithelial-mesenchymal transition in tissue repair and fibrosis. Cell Tissue Res 2016;365:495–506
33. Khan MA, Palaniyar N. Transcriptional firing helps to drive NETosis. Sci Rep 2017;7:41749
34. Liu C, Lim ST, Teo MHY, et al. Collaborative regulation of LRG1 by TGF-β1 and PPAR-β/δ modulates chronic pressure overload-induced cardiac fibrosis. Circ Heart Fail 2019;12:e005962
35. Druhan LJ, Lance A, Li S, et al. Leucine rich α-2 glycoprotein: a novel neutrophil granule protein and modulator of myelopoiesis. PLoS One 2017;12:e0170261
36. Kumagai S, Nakayama H, Fujimoto M, et al. Myeloid cell-derived LRG attenuates adverse cardiac remodelling after myocardial infarction. Cardiovasc Res 2016;109:272–282
37. O'Donnell LC, Druhan LJ, Avalos BR. Molecular characterization and expression analysis of leucine-rich alpha2-glycoprotein, a novel marker of granulocytic differentiation. J Leukoc Biol 2002;72:478–485
38. Gerdes J, Lemke H, Baisch H, Wacker HH, Schwab U, Stein H. Cell cycle analysis of a cell proliferation-associated human nuclear antigen defined by the monoclonal antibody Ki-67. J Immunol 1984;133:1710–1715
39. Salic A, Mitchison TJ. A chemical method for fast and sensitive detection of DNA synthesis in vivo. Proc Natl Acad Sci U S A 2008;105:2415–2420
40. Zhou Y, Zhang X, Zhang J, Fang J, Ge Z, Li X. LRG1 promotes proliferation and inhibits apoptosis in colorectal cancer cells via RUNX1 activation. PLoS One 2017;12:e0175122
41. Li Z, Zeng C, Nong Q, et al. Exosomal leucine-rich-alpha2-glycoprotein 1 derived from non-small-cell lung cancer cells promotes angiogenesis via TGF-β signal pathway. Mol Ther Oncolytics 2019;14:313–322
42. Yan C, Grimm WA, Garner WL, et al. Epithelial to mesenchymal transition in human skin wound healing is induced by tumor necrosis factor-alpha through bone morphogenic protein-2. Am J Pathol 2010;176:2247–2258
43. Okonkwo UA, DiPietro LA. Diabetes and wound angiogenesis. Int J Mol Sci 2017;18:1419

44. Goumans MJ, Valdimarsdottir G, Itoh S, et al. Activin receptor-like kinase (ALK)1 is an antagonistic mediator of lateral TGFbeta/ALK5 signaling. Mol Cell 2003;12:817–828
45. Loots MA, Lamme EN, Zeegelaar J, Mekkes JR, Bos JD, Middelkoop E. Differences in cellular infiltrate and extracellular matrix of chronic diabetic and venous ulcers versus acute wounds. J Invest Dermatol 1998;111:850–857
46. Zhong D, He G, Zhao S, et al. LRG1 modulates invasion and migration of glioma cell lines through TGF-β signaling pathway. Acta Histochem 2015;117:551–558
47. Urushima H, Fujimoto M, Mishima T, et al. Leucine-rich alpha 2 glycoprotein promotes Th17 differentiation and collagen-induced arthritis in mice through enhancement of TGF-β-Smad2 signaling in naïve helper T cells. Arthritis Res Ther 2017;19:137